Valence Bond Orders at Charge Neutrality in a Possible Two-Orbital Extended Hubbard Model for Twisted Bilayer Graphene

Yuan Da Liao,[1,2] Zi Yang Meng,[3,1,4,5] and Xiao Yan Xu[6,7,*]

[1]Beijing National Laboratory for Condensed Matter Physics and Institute of Physics, Chinese Academy of Sciences, Beijing 100190, China
[2]School of Physical Sciences, University of Chinese Academy of Sciences, Beijing 100190, China
[3]Department of Physics and HKU-UCAS Joint Institute of Theoretical and Computational Physics, The University of Hong Kong, Pokfulam Road, Hong Kong, China
[4]Songshan Lake Materials Laboratory, Dongguan, Guangdong 523808, China
[5]CAS Center of Excellence in Topological Quantum Computation and School of Physical Sciences, University of Chinese Academy of Sciences, Beijing 100190, China
[6]Department of Physics, Hong Kong University of Science and Technology, Clear Water Bay, Hong Kong, China
[7]Department of Physics, University of California at San Diego, La Jolla, California 92093, USA

(Received 11 February 2019; published 8 October 2019)

An extended Hubbard model on a honeycomb lattice with two orbitals per site at charge neutrality is investigated with unbiased large-scale quantum Monte Carlo simulations. The Fermi velocity of the Dirac fermions is renormalized as the cluster charge interaction increases, until a mass term emerges and a quantum phase transition from Dirac semimetal to valence bond solid (VBS) insulator is established. The quantum critical point is discovered to belong to the 3D $N = 4$ Gross-Neveu chiral XY universality with the critical exponents obtained at high precision. Further enhancement of the interaction drives the system into two different VBS phases, the properties and transition between them are also revealed. Since the model is related to magic-angle twisted bilayer graphene, our results may have relevance towards the symmetry breaking order at the charge neutrality point of the material, and associate the wide range of universal strange metal behavior around it with quantum critical fluctuations.

DOI: 10.1103/PhysRevLett.123.157601

Introduction.—Twisted bilayer graphene (TBG) forms moiré patterns in real space with the size of the moiré unit cell tuned by the twisting angle. The Fermi velocity of the Dirac fermions of monolayer graphene is renormalized in TBG. At some magic angle, the Fermi velocity vanishes [1–6], such that flat bands are formed and the system consequently become susceptible towards many instabilities. In 2018, the gate tunable magic-angle TBG was realized in the laboratory [7,8], and interesting phenomena encompassing the correlated insulating phase [7], unconventional superconductivity [8,9] and strange metal behavior [10] were quickly discovered. Those results hint that, unlike its monolayer cousin, the gate tunable magic-angle TBG is a strongly correlated system in nature and shares many common features of the phase diagram of doped cuprates; consequently, this has spurred the interest of theoretical and experimental communities on moiré physics [9–40].

Compared with cuprates, magic-angle TBG also acquires unique properties and two of them are related with the modeling of the material. First, although there are huge numbers of electrons in one unit cell which fill thousands of energy bands, various band calculations show that there exists an isolated band branch with four bands around the charge neutrality point [1–5,23,27]. The four bands are made up of the spin and valley degrees of freedom of untwisted graphene. Second, the charge center forms a triangular lattice, but symmetry obstacles force one to define the effective model on a honeycomb lattice if the different band degeneracy at Γ and $\mathbf{K}$ of the BZ are to be respected [13,14]. Meanwhile, there are also obstacles from deriving a single valley tight-binding model due to chirality or mirror symmetry [26]. Putting all these factors together, a two orbital (counts the two valleys of the untwisted graphene) spinful lattice model on a honeycomb lattice with cluster charge interaction (considering the charge center form triangle lattice) is a good starting point to describe the system [14,21,23,41].

But such a model is still a strongly correlated one and cannot be solved analytically. In light of the situation, we performed unbiased sign-problem-free quantum Monte Carlo (QMC) simulation to investigate such a system at charge neutrality and map out its precise phase diagram. By gradually increasing the interaction strength, the phase diagram exhibits—in a consecutive manner—a Dirac semi-metal (DSM), a plaquette valence bond solid (pVBS), and a columnar valence bond solid (cVBS) phase at weak, intermediate, and strong interaction

regions. The quantum phase transitions between these phases are revealed with scrutiny and we found the DSM-pVBS transition is continuous, belonging to the 3D $N = 4$ Gross-Neveu chiral XY universality class; the pVBS-cVBS transition on the other hand is first order but bestowed with a sign change in the mass term of a fermion bilinear, and implies that a quantum pseudospin Hall effect can be generated between the zigzag domains of those two insulators. The experimental relevance of our discoveries in quantum criticality and phase transitions towards on-going investigations of TBGs is also discussed.

Model and method.—We study an extended Hubbard model with two orbitals of spinful fermions on a honeycomb lattice. The model contains two parts, $H = H_0 + H_U$, where

$$H_0 = -t\sum_{\langle ij\rangle l\sigma}(c^\dagger_{il\sigma}c_{jl\sigma} + \text{H.c.}) - t_2\sum_{\langle ij\rangle' l\sigma}(i^{2l-1}c^\dagger_{il\sigma}c_{jl\sigma} + \text{H.c.}) \tag{1}$$

is the tight-binding part introduced in Ref. [23] and serves as a minimal model to describe the low energy band structure of magic-angle TBG with Dirac points at charge neutrality and band splitting along the Γ-M direction. Here $c^\dagger_{il\sigma}$ ($c_{il\sigma}$) is the creation (annihilation) operator of the electron at site i, orbital $l = 1, 2$ with spin $\sigma = \uparrow, \downarrow$. Throughout this Letter, we take the nearest neighbor hopping t as the energy unit. The fifth neighbor hopping (it_2 for $l = 1$ and $-it_2$ for $l = 2$) is purely imaginary and breaks orbital degeneracy along the $\Gamma - M$ direction. As t_2/t is small in the material, we focus on the range of $t_2/t < 0.6$.

For the Coulomb interaction term H_U, as the Wannier orbitals are quite extended in TBG, onsite, first, second and third neighbor repulsions are all important [14,23,41]. To capture such nonlocal interactions, a cluster charge Hubbard term which maintains the average filling of each elemental hexagon on the honeycomb lattice to be 4 is the genuine choice; therefore we write down

$$H_U = U\sum_{\hexagon}(Q_{\hexagon} - 4)^2, \tag{2}$$

where the cluster charge $Q_{\hexagon} \equiv \sum_{i\in\hexagon}(n_i/3)$ with $n_i = \sum_{l\sigma} c^\dagger_{il\sigma}c_{il\sigma}$ summing over all the six sites of the elemental hexagon. If we expand Eq. (2), the onsite, first, second, and third neighbor interaction strengths are $\frac{2}{3}U$, $\frac{4}{9}U$, $\frac{2}{9}U$, and $\frac{2}{9}U$, with ratio 3:2:1:1. As a different range of interactions favors different kinds of order, it may require a larger interaction to open a fermion gap compared to a local Hubbard model.

At any finite U/t, the model $H = H_0 + H_U$ is nonperturbative in nature, but we found it actually immune from the sign problem due to an antiunitary symmetry [42] at the charge neutrality point, and it is readily exposed to large-scale projection QMC (PQMC) simulations [43–45]. PQMC simulations seek out the ground state phase diagram, correlation functions (to determine the pattern of symmetry breaking), and dynamical information (single-particle and collective excitation gaps above the ground state), and has been employed in several of our previous studies [21,46–48]. The symmetry analysis and numeric implementation of PQMC simulations are discussed in the Supplemental Material [49]; we only mention here that the projection length is set to $\Theta = 2L$ and the simulations are performed with linear system size up to $L = 24$, which amounts to $N_e = 4 \times L^2 = 2304$ interacting electrons on the TBG model.

Phase diagram and quantum criticality.—Our phase diagram, expanded by axes U/t and t_2/t, is shown in Fig. 1, the DSM, pVBS, and cVBS phases are in place. The two VBSs are gapped insulators. In the following parts, $t_2/t = 0$ if it is not specified. It is interesting to notice that different from the local Hubbard model [46,50], $t - J$ [51] and the extended cluster charge models with single orbital [21] on honeycomb lattice, the AB sublattice antiferromagnetic insulating phase is suppressed in our phase diagram even at very large U/t, which may be understood by a perturbation theory in the large U/t limit [52], but the existence of two VBS phases in such a simple model is unexpected and has not been found in a local Hubbard model before.

To study the DSM-pVBS transition, we measure the bond-bond structure factor,

$$C_B(\mathbf{k}) = \frac{1}{L^4}\sum_{i,j} e^{i\mathbf{k}\cdot(\mathbf{r}_i - \mathbf{r}_j)}\langle B_{i,\delta}B_{j,\delta}\rangle, \tag{3}$$

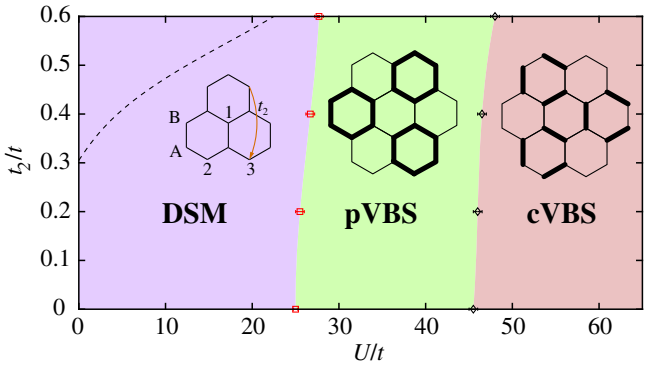

FIG. 1. Ground state phase diagram. As a function of U/t, the DSM, pVBS, and cVBS phases reveal themselves. The fifth neighbor hopping strength t_2 is marked as an orange line in the inset. Inside DSM, the t_2/t ratio modifies the band degeneracy and Fermi surface topology, and the black dashed line signifies the corresponding band structure crossover, where excitons formed between orbitals might condense. The different patterns of the valence bonds are shown in the insets. The DSM-pVBS transition is continuous and shown to belong to the 3D $N = 4$ chiral XY Gross-Neveu universality. The pVBS-cVBS transition is first order, but could carry topological edge states in terms of the quantum pseudospin Hall effect in the pVBS-cVBS zigzag domain wall.

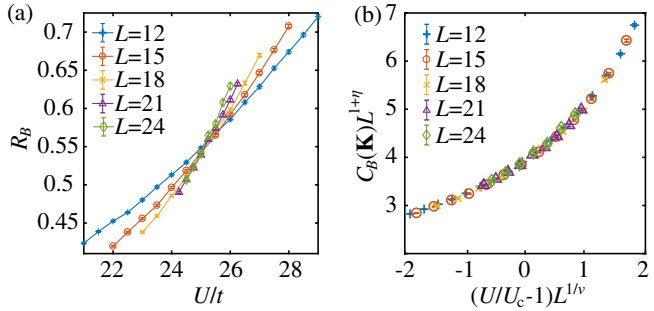

FIG. 2. (a) The bond-bond correlation ratio R_B and (b) data collapse analysis of the structure factor $C_B(\mathbf{K})$ at $t_2/t = 0$ as a function of U/t with $L = 12, 15, \ldots, 24$. The crossing of R_B in (a) gives the DSM-pVBS critical point $U_c/t = 25.1(2)$. The data collapse in (b) gives the 3D $N = 4$ Gross-Neveu chiral XY exponents $\eta = 0.80(2)$, $\nu = 1.01(3)$.

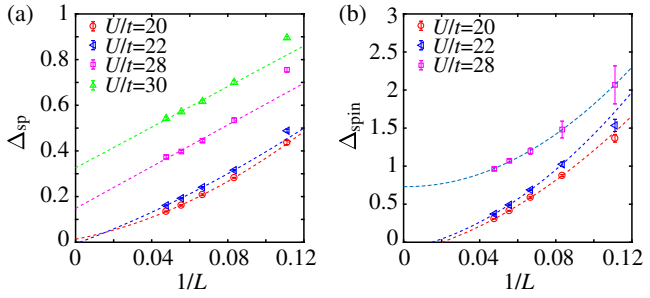

FIG. 3. (a) The $1/L$ extrapolation of the single-particle gap $\Delta_{sp}(\mathbf{K})$, the gap opens between $U/t = 22$ and $U/t = 28$, consistent with the U_c/t obtained from the bond correlation ratio in Fig. 2(a). (b) The $1/L$ extrapolation of spin gap $\Delta_{spin}(\mathbf{K})$, the spin gap opens hand in hand with the single-particle gap as the establishment of pVBS order.

where bond operator $B_{i,\delta} = \sum_{l,\alpha}(c^\dagger_{i,l,\alpha}c_{i+\delta,l,\alpha} + \text{H.c.})$ with δ standing for one of the three nearest-neighbor bond directions ($\hat{e_1}$, $\hat{e}_2$ and $\hat{e}_3$) and $\hat{e}_1$ is chosen in the calculation. Results show that $C_B(\mathbf{k})$ is peaked at momenta $\mathbf{K}$ and $\mathbf{K}'$ $[\pm(4\pi/3\sqrt{3}a_0), 0]$ of the BZ suggesting the VBS patterns shown in the inset of Fig. 1.

To locate the DSM-pVBS transition point, we plot the correlation ratio $R_B(U, L) = 1 - \{[C_B(\mathbf{K} + \delta\mathbf{q})]/C_B(\mathbf{K})\}$ for different U and system size L with $|\delta\mathbf{q}| \sim (1/L)$. This quantity approaches to one (zero) in an ordered (disordered) phase, and implies a crossing for different L at a critical point [53] as shown in Fig. 2(a), where one reads $U_c/t = 25.1(2)$. We further collapse the bond-bond structure factor with scaling relation $C_B(\mathbf{K}, U, L) = L^{-(1+\eta)}f(L^{1/\nu}(U - U_c)/U_c)$ (dynamical exponent z is set to 1 due to Lorentz symmetry of massless Dirac fermions), as shown in Fig. 2(b). and we obtain the critical exponents $\eta = 0.80(2)$ and $\nu = 1.01(3)$. Since our Dirac fermions acquire 4 degrees of freedom per site and the pVBS phase contains an emergent $U(1)$ symmetry close to the DSM-pVBS transition as shown in Refs. [21,52], we identify this transition in the 3D $N = 4$ Gross-Nevue chiral XY universality class [52,54–64]. The critical exponents obtained here $[\eta = 0.80(2), \nu = 1.01(3)]$ are comparable with those calculated theoretically or numerically in the literature, as shown in Table I of the Supplemental Material [49].

Gapped phases: cVBS and pVBS.—The DSM is known to possess robust massless linear dispersion at weak interaction ($U < U_c$) [21,50,52,65–68] and the Dirac fermion will be gapped out in the pVBS insulator. To monitor the opening of the single-particle gap across the DSM-pVBS transition, we measure the dynamical single-particle Green's function and follow its decay in imaginary time $G(\mathbf{k}, \tau) \propto e^{-\Delta_{sp}(\mathbf{k})\tau}$ at momentum $\mathbf{K}$ for increasing system size L and imaginary time displacement τ, with $G(\mathbf{k},\tau)=(1/4L^2)\sum_{i,j,l,\sigma}e^{i\mathbf{k}\cdot(\mathbf{r}_i-\mathbf{r}_j)}\langle c_{i,l,\sigma}(\tau/2)c^\dagger_{j,l,\sigma}[-(\tau/2)]\rangle$. The obtained Δ_{sp} for different interaction U and L are shown in Fig. 3(a). It is clear that when $U < U_c$, $\Delta_{sp} \to 0$ and when $U > U_c$, Δ_{sp} goes to a finite value, which validate the picture that the DSM-pVBS transition is accompanied by the opening of the single-particle gap.

The VBS phase is related with the formation of a spin singlet, either within the hexagon plaquette (pVBS) or along the nearest-neighbor bond (cVBS), and to see that one can examine the spin excitation gap, obtained from the imaginary time decay of dynamical spin-spin correlation function $C_S(\mathbf{q}, \tau) = (1/N)\sum_{i,j} e^{i\mathbf{q}\cdot(\mathbf{r}_i-\mathbf{r}_j)}\langle \mathbf{S}_i(\tau/2)\mathbf{S}_j[-(\tau/2)]\rangle$ as $C_S(\mathbf{K}, \tau) \propto e^{-\Delta_{spin}(\mathbf{K})\tau}$. The spin operator is defined as $\mathbf{S}_i = \frac{1}{2}\sum_{l,\alpha,\beta} c^\dagger_{i,l,\alpha}(\boldsymbol{\sigma})_{\alpha,\beta}c_{i,l,\beta}$ for the $t_2/t \neq 0$ case with $\boldsymbol{\sigma} = (\sigma^1, \sigma^2, \sigma^3)$, and $(\mathbf{S}_i)^\nu_\mu = c^\dagger_{i,\mu}c_{i,\nu} - (\delta_{\mu\nu}/4)\sum_{\rho=1}^4 c^\dagger_{i,\rho}c_{i,\rho}$ for the $t_2/t = 0$ case where μ, ν, and ρ denote a combination of indexes of spin and orbital as components of the SU(4) generator. Similar to the case of the single-particle gap, after extrapolation of $\Delta_{spin}(\mathbf{K})$ (Δ_{spin} is the smallest and degenerate at momenta $\mathbf{K}$, $\mathbf{K}'$ and Γ) for various L and U, one can see from Fig. 3(b) that the spin gap is also zero when $U < U_c$ in the DSM phase and becomes finite when $U > U_c$ as the system enters the pVBS phase.

Further increasing U/t from the pVBS phase, a kinetic energy jump at $U/t \approx 46$ is observed, as shown in Fig. 4(a). At the same time, the VBS correlation $C_B(\mathbf{K})$ also acquires a jump at the same U as shown in Fig. 4(b). These results point out that, besides $U_c/t = 25.1(2)$, there is another first order phase transition at $U_{VBS}/t \approx 46$ between two different VBS phases. There are three nonequivalent VBS configurations, but only two of them, the pVBS and cVBS as depicted in the inset of Fig. 1, can perturbatively open the single-particle gap to VBS phases. And the jumps observed in Figs. 4(a) and 4(b) might be the transition between these two VBS phases.

To verify this idea, we follow Refs. [51,52] and make use of the nearest-neighboring bonds $B_{i,\delta}$ originated from sublattice A to construct complex order parameters $D_{\mathbf{K}} = (1/L^2)\sum_i(B_{i,\hat{e}_1} + \omega B_{i,\hat{e}_2} + \omega^2 B_{i,\hat{e}_3})e^{i\mathbf{K}\cdot\mathbf{r}_i}$ with $\omega = e^{i(2\pi/3)}$.

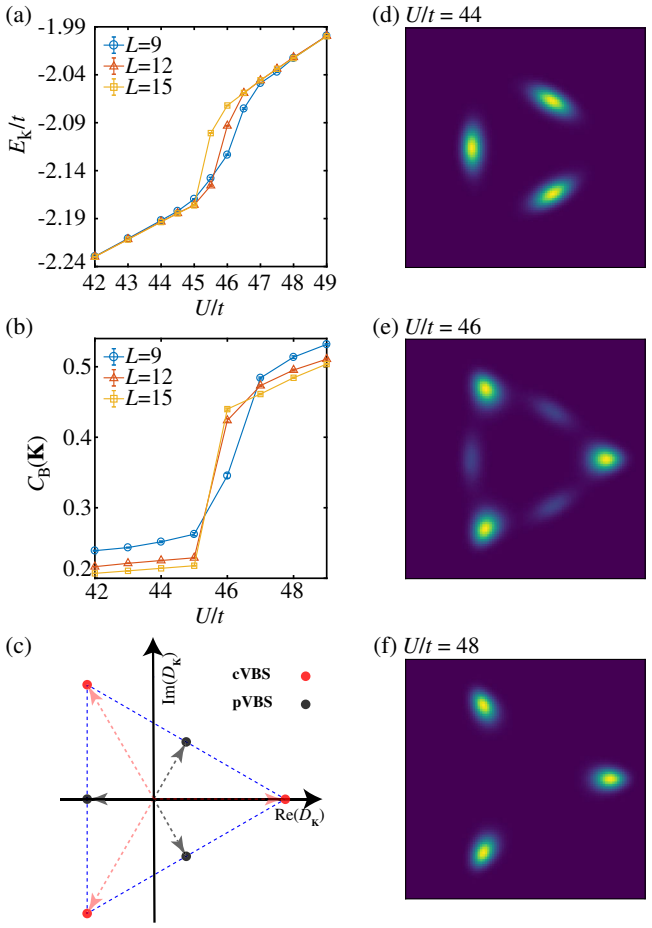

FIG. 4. (a) Kinetic energy per site of the system for U at large values. The sharp jump signifies a first order transition. (b) $C_B(\mathbf{K})$ for the same process, a jump in VBS order is also observed, suggesting this is a transition between different VBS phases. (c) Angular dependence of the complex order parameter $D_{\mathbf{K}}$. Black dots represent ideal pVBS order, and red dots represent ideal cVBS order. (d)–(e) Histogram of $D_{\mathbf{K}}$ at different interaction strengths $U < U_{\mathrm{VBS}}$, $U \approx U_{\mathrm{VBS}}$, and $U > U_{\mathrm{VBS}}$.

The Monte Carlo histogram of $D_{\mathbf{K}}$ can reveal the difference between the two VBS phases, as shown in Fig. 4(c). The angular distribution of pVBS will peak at $\arg(D_{\mathbf{K}}) = (\pi/3), \pi, (5\pi/3)$, whereas that of cVBS will peak at $\arg(D_{\mathbf{K}}) = 0, (2\pi/3), (4\pi/3)$. Figures 4(d), 4(e), and 4(f) show the corresponding histograms at three representative interaction strengths $U = 44t < U_{\mathrm{VBS}}$, $U = 46t \approx U_{\mathrm{VBS}}$, $U = 48t > U_{\mathrm{VBS}}$. It is clear that Figs. 4(d) and 4(f) are inside pVBS and cVBS, respectively, Fig. 4(e), on the other hand, depicts the distribution of both characters, a typical example of the coexistence at the first order transition point. In this way, the two VBS phases and their first order transition are clearly established. A similar scenario, between two Kekulé patterned superconducting states, in the context of attractive interaction on honeycomb lattice has been discussed in Ref. [69].

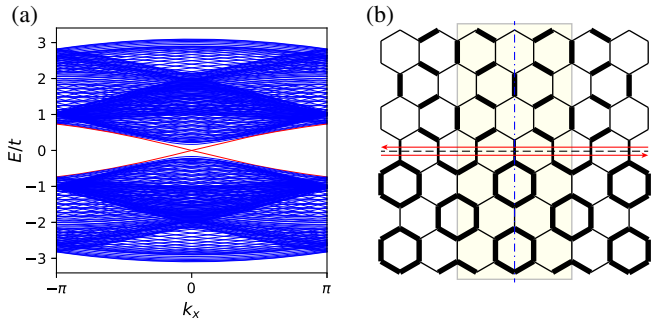

FIG. 5. (a) Spectrum of the zigzag domain wall of pVBS and cVBS. The red line denotes the helical edge states. In the calculation, both the width of pVBS and cVBS strips are set to 24 times the honeycomb unit cell. (b) The zigzag domain wall of pVBS and cVBS with the bottom part the pVBS phase and top part the cVBS phase. The hopping strength is $-1.1t$ for strong bonds and $-0.9t$ for weak bonds. The pVBS and cVBS are connected by vertical bonds with hopping strength $-t$. The domain wall has periodic boundary condition along the x direction, and is put on a torus (the upper boundary and lower boundary are also connected by vertical bonds with hopping strength $-t$). The shaded region denotes the super unit cell of the domain wall.

Pseudo spin Hall effect in zigzag domain of pVBS and cVBS.—Our model provides the unique opportunity that pVBS and cVBS all appear in the phase diagram due to spontaneous Dirac mass generation, and one can reveal their connection with the following analysis. In the VBS phase we consider a mean field description with bond charge order, and suppress the spin and orbital degrees of freedom for the moment. Then the static VBS order becomes a modulation in the nearest neighbor hopping. As shown in the inset of Fig. 1, there are two kinds of bonds and the hopping magnitude is defined as $(1+\delta)t$ and $(1-\delta)t$. From a tight binding Hamiltonian with such bond modulation, a 4×4 $k \cdot p$ Hamiltonian at the Γ point can be derived,

$$H_{\mathrm{eff}}(\mathbf{k}) = -t(\tilde{\mathbf{k}} \cdot \tilde{\mathbf{s}}\tau^2 + ms^0\tau^3), \tag{4}$$

where momentum $\tilde{\mathbf{k}} \equiv [(3/2)k_y, (\sqrt{3}/2)ik_x, \sqrt{3}k_x]$, the vector $\tilde{\mathbf{s}} = (s^1, s^2, s^3)$ and mass term $m = 2\delta$. Here s^i and τ^i are Pauli matrices in two different spaces. From the $k \cdot p$ Hamiltonian, it is clear that the bond modulation plays the role of a mass term, and there is a sign change in it across the pVBS-cVBS transition.

The sign change in the mass term motivates us to study the domain walls between the pVBS and cVBS phases. Both VBS phases coexist at the first order transition point and may go through a gap close to the domain wall. Interestingly, the calculation of the spectrum of the pVBS and cVBS zigzag domain wall on a torus shows that there exist robust helical edge states as depicted in Fig. 5. Such edge states are protected by the combined symmetry of the

sublattice (chiral) and mirror [along a bond with the mirror plane denoted by the blue dashed line in Fig. 5(b)] and can be interpreted as the edge states of the quantum pseudospin Hall effect [70–72].

Experimental relevance.—Recent STM experiments [73,74] find significant gap opening near charge neutrality point (CNP) indicating symmetry breaking order. The insulating phase at CNP is also found in many other experiments [9,10,40]. The spontaneous symmetry breaking VBS phases found in our simulations hence provide good candidates, and a Fourier transform of the large-area STM topograph may detect additional features at the wavelength of VBS [75]. Although an exact estimation of cluster charge interaction U/t is not easy, our results hint at the possibility that magic-angle TBG is close to a QCP where the Dirac mass is spontaneously generated and opens the charge neutrality gap. Other exciting observations show a wide range of strange metal behavior, whose existence seems robust against experimental details [10]. Such universal transport behavior is the hallmark of quantum critical phenomena, possibly originated from the 3D Gross-Neveu chiral XY transition between DSM and pVBS discovered here. Moreover, the strange metal behavior is pronounced near $\pm 1/4$ filling, and not well established near the charge neutrality point; this is consistent with the picture that the charge neutrality point is gapped but close to the QCP—when gated, the quantum critical fluctuation kicks in and generates strange metal behavior. A final remark is that the model we studied assumed well-defined valley degrees of freedom (in terms of two orbitals). Actually, if the valleys' coupling is considered in TBG, it will give a single orbital model [14]. The interesting thing is that we still find a QCP at moderate interaction strength in the single orbital model that may be related to the intriguing physics near $\pm 1/4$ filling of magic-angle TBG [21].

We thank Noah Yuan, Liang Fu, Eslam Khalaf, Lukas Janssen, Yang Qi, Qing-Rui Wang, Chen Fang, K. T. Law, and Patrick Lee for helpful discussions. We thank Michael Scherer for providing us the $4-\epsilon$ four loop calculation of critical exponents for the 3D $N=4$ Gross-Neveu chiral XY universality class. Y. D. L. and Z. Y. M. acknowledge support from the Ministry of Science and Technology of China through the National Key Research and Development Program (2016YFA0300502), the Strategic Priority Research Program of the Chinese Academy of Sciences (XDB28000000), the National Science Foundation of China (11574359) and Research Grants Council of Hong Kong Special Administrative Region of China through 17303019. X. Y. X. is thankful for the support of Research Grants Council of Hong Kong Special Administrative Region of China through C6026-16W. We thank the Center for Quantum Simulation Sciences at Institute of Physics, Chinese Academy of Sciences, and the Tianhe-1A platform at the National Supercomputer Center in Tianjin and the Tianhe-2 platform at the National Supercomputer Center in Guangzhou for technical support and generous allocation of CPU time.

*wanderxu@gmail.com

[1] R. Bistritzer and A. H. MacDonald, Proc. Natl. Acad. Sci. U.S.A. **108**, 12233 (2011).
[2] E. Suárez Morell, J. D. Correa, P. Vargas, M. Pacheco, and Z. Barticevic, Phys. Rev. B **82**, 121407(R) (2010).
[3] J. M. B. Lopes dos Santos, N. M. R. Peres, and A. H. Castro Neto, Phys. Rev. B **86**, 155449 (2012).
[4] S. Fang and E. Kaxiras, Phys. Rev. B **93**, 235153 (2016).
[5] G. Trambly de Laissardière, D. Mayou, and L. Magaud, Phys. Rev. B **86**, 125413 (2012).
[6] G. Tarnopolsky, A. J. Kruchkov, and A. Vishwanath, Phys. Rev. Lett. **122**, 106405 (2019).
[7] Y. Cao, V. Fatemi, A. Demir, S. Fang, S. L. Tomarken, J. Y. Luo, J. D. Sanchez-Yamagishi, K. Watanabe, T. Taniguchi, E. Kaxiras, R. C. Ashoori, and P. Jarillo-Herrero, Nature (London) **556**, 80 (2018).
[8] Y. Cao, V. Fatemi, S. Fang, K. Watanabe, T. Taniguchi, E. Kaxiras, and P. Jarillo-Herrero, Nature (London) **556**, 43 (2018).
[9] M. Yankowitz, S. Chen, H. Polshyn, Y. Zhang, K. Watanabe, T. Taniguchi, D. Graf, A. F. Young, and C. R. Dean, Science **363**, 1059 (2019).
[10] Y. Cao, D. Chowdhury, D. Rodan-Legrain, O. Rubies-Bigordà, K. Watanabe, T. Taniguchi, T. Senthil, and P. Jarillo-Herrero, arXiv:1901.03710.
[11] G. Chen, L. Jiang, S. Wu, B. Lv, H. Li, K. Watanabe, T. Taniguchi, Z. Shi, Y. Zhang, and F. Wang, Nat. Phys. **15**, 237 (2019).
[12] C. Xu and L. Balents, Phys. Rev. Lett. **121**, 087001 (2018).
[13] N. F. Q. Yuan and L. Fu, Phys. Rev. B **98**, 045103 (2018).
[14] H. C. Po, L. Zou, A. Vishwanath, and T. Senthil, Phys. Rev. X **8**, 031089 (2018).
[15] H. C. Po, L. Zou, T. Senthil, and A. Vishwanath, Phys. Rev. B **99**, 195455 (2019).
[16] C.-C. Liu, L.-D. Zhang, W.-Q. Chen, and F. Yang, Phys. Rev. Lett. **121**, 217001 (2018).
[17] J. F. Dodaro, S. A. Kivelson, Y. Schattner, X. Q. Sun, and C. Wang, Phys. Rev. B **98**, 075154 (2018).
[18] T. Huang, L. Zhang, and T. Ma, Sci. Bull. **64**, 310 (2019).
[19] B. Roy and V. Juričić, Phys. Rev. B **99**, 121407(R) (2019).
[20] H. Guo, X. Zhu, S. Feng, and R. T. Scalettar, Phys. Rev. B **97**, 235453 (2018).
[21] X. Y. Xu, K. T. Law, and P. A. Lee, Phys. Rev. B **98**, 121406 (R) (2018).
[22] Y.-H. Zhang, D. Mao, Y. Cao, P. Jarillo-Herrero, and T. Senthil, Phys. Rev. B **99**, 075127 (2019).
[23] M. Koshino, N. F. Q. Yuan, T. Koretsune, M. Ochi, K. Kuroki, and L. Fu, Phys. Rev. X **8**, 031087 (2018).
[24] F. Wu, A. H. MacDonald, and I. Martin, Phys. Rev. Lett. **121**, 257001 (2018).
[25] Q. K. Tang, L. Yang, D. Wang, F. C. Zhang, and Q. H. Wang, Phys. Rev. B **99**, 094521 (2019).
[26] L. Zou, H. C. Po, A. Vishwanath, and T. Senthil, Phys. Rev. B **98**, 085435 (2018).
[27] J. Kang and O. Vafek, Phys. Rev. X **8**, 031088 (2018).

[28] A. Thomson, S. Chatterjee, S. Sachdev, and M. S. Scheurer, Phys. Rev. B **98**, 075109 (2018).
[29] J. W. F. Venderbos and R. M. Fernandes, Phys. Rev. B **98**, 245103 (2018).
[30] G.-Y. Zhu, T. Xiang, and G.-M. Zhang, Sci. Bull. **63**, 1087 (2018).
[31] L. Zhang, Sci. Bull. **64**, 495 (2019).
[32] Y.-Z. You and A. Vishwanath, arXiv:1805.06867.
[33] B. Lian, Z. Wang, and B. A. Bernevig, Phys. Rev. Lett. **122**, 257002 (2019).
[34] Z. Song, Z. Wang, W. Shi, G. Li, C. Fang, and B. A. Bernevig, Phys. Rev. Lett. **123**, 036401 (2019).
[35] J. Liu, J. Liu, and X. Dai, Phys. Rev. B **99**, 155415 (2019).
[36] M. Xie and A. H. MacDonald, arXiv:1812.04213.
[37] Z. Zhu, D. Sheng, and L. Fu, Phys. Rev. Lett. **123**, 087602 (2019).
[38] C. Shen, N. Li, S. Wang, Y. Zhao, J. Tang, J. Liu, J. Tian, Y. Chu, K. Watanabe, T. Taniguchi, R. Yang, Z. Y. Meng, D. Shi, and G. Zhang, arXiv:1903.06952.
[39] X. Liu, Z. Hao, E. Khalaf, J. Y. Lee, K. Watanabe, T. Taniguchi, A. Vishwanath, and P. Kim, arXiv:1903.08130.
[40] X. Lu, P. Stepanov, W. Yang, M. Xie, M. A. Aamir, I. Das, C. Urgell, K. Watanabe, T. Taniguchi, G. Zhang, A. Bachtold, A. H. MacDonald, and D. K. Efetov, arXiv:1903.06513.
[41] J. Kang and O. Vafek, Phys. Rev. Lett. **122**, 246401 (2019).
[42] C. Wu and S.-C. Zhang, Phys. Rev. B **71**, 155115 (2005).
[43] R. Blankenbecler, D. J. Scalapino, and R. L. Sugar, Phys. Rev. D **24**, 2278 (1981).
[44] J. E. Hirsch, Phys. Rev. B **31**, 4403 (1985).
[45] F. Assaad and H. Evertz, World-line and determinantal quantum Monte Carlo methods for spins, phonons and electrons, in *Computational Many-Particle Physics*, edited by H. Fehske, R. Schneider, and A. Weiße (Springer, Berlin, Heidelberg, 2008), pp. 277–356.
[46] Z. Y. Meng, T. C. Lang, S. Wessel, F. F. Assaad, and A. Muramatsu, Nature (London) **464**, 847 (2010).
[47] X. Y. Xu, K. S. D. Beach, K. Sun, F. F. Assaad, and Z. Y. Meng, Phys. Rev. B **95**, 085110 (2017).
[48] Y.-Y. He, X. Y. Xu, K. Sun, F. F. Assaad, Z. Y. Meng, and Z.-Y. Lu, Phys. Rev. B **97**, 081110(R) (2018).
[49] See Supplemental Material at http://link.aps.org/supplemental/10.1103/PhysRevLett.123.157601 for detailed discussions of the tight-binding model of the TBG, its dispersion and the fermiology at various t_2/t, the symmetry analysis of the model and absence of sign-problem and its PQMC implementations, derivation of the $k \cdot p$ Hamiltonian for the VBS phase, and the critical properties of the $N = 4$ Gross-Neveu chiral XY transition.
[50] S. Sorella and E. Tosatti, Europhys. Lett. **19**, 699 (1992).
[51] T. C. Lang, Z. Y. Meng, A. Muramatsu, S. Wessel, and F. F. Assaad, Phys. Rev. Lett. **111**, 066401 (2013).
[52] Z. Zhou, D. Wang, Z. Y. Meng, Y. Wang, and C. Wu, Phys. Rev. B **93**, 245157 (2016).
[53] R. K. Kaul, Phys. Rev. Lett. **115**, 157202 (2015).
[54] D. J. Gross and A. Neveu, Phys. Rev. D **10**, 3235 (1974).
[55] S. Hands, A. Kocic, and J. Kogut, Ann. Phys. (N.Y.) **224**, 29 (1993).
[56] B. Rosenstein, H.-L. Yu, and A. Kovner, Phys. Lett. B **314**, 381 (1993).
[57] N. Zerf, L. N. Mihaila, P. Marquard, I. F. Herbut, and M. M. Scherer, Phys. Rev. D **96**, 096010 (2017).
[58] Z.-X. Li, Y.-F. Jiang, S.-K. Jian, and H. Yao, Nat. Commun. **8**, 314 (2017).
[59] M. M. Scherer and I. F. Herbut, Phys. Rev. B **94**, 205136 (2016).
[60] L. N. Mihaila, N. Zerf, B. Ihrig, I. F. Herbut, and M. M. Scherer, Phys. Rev. B **96**, 165133 (2017).
[61] S.-K. Jian and H. Yao, Phys. Rev. B **96**, 195162 (2017).
[62] L. Classen, I. F. Herbut, and M. M. Scherer, Phys. Rev. B **96**, 115132 (2017).
[63] E. Torres, L. Classen, I. F. Herbut, and M. M. Scherer, Phys. Rev. B **97**, 125137 (2018).
[64] B. Ihrig, L. N. Mihaila, and M. M. Scherer, Phys. Rev. B **98**, 125109 (2018).
[65] F. F. Assaad and I. F. Herbut, Phys. Rev. X **3**, 031010 (2013).
[66] Y. Otsuka, S. Yunoki, and S. Sorella, Phys. Rev. X **6**, 011029 (2016).
[67] T. Sato, M. Hohenadler, and F. F. Assaad, Phys. Rev. Lett. **119**, 197203 (2017).
[68] C. Chen, X. Y. Xu, Z. Y. Meng, and M. Hohenadler, Phys. Rev. Lett. **122**, 077601 (2019).
[69] B. Roy and I. F. Herbut, Phys. Rev. B **82**, 035429 (2010).
[70] T. Kariyado and X. Hu, Sci. Rep. **7**, 16515 (2017).
[71] Y. Liu, C.-S. Lian, Y. Li, Y. Xu, and W. Duan, Phys. Rev. Lett. **119**, 255901 (2017).
[72] S. Sorella, K. Seki, O. O. Brovko, T. Shirakawa, S. Miyakoshi, S. Yunoki, and E. Tosatti, Phys. Rev. Lett. **121**, 066402 (2018).
[73] A. Kerelsky, L. McGilly, D. M. Kennes, L. Xian, M. Yankowitz, S. Chen, K. Watanabe, T. Taniguchi, J. Hone, C. Dean, A. Rubio, and A. N. Pasupathy, Nature (London) **572**, 95 (2019).
[74] Y. Choi, J. Kemmer, Y. Peng, A. Thomson, H. Arora, R. Polski, Y. Zhang, H. Ren, J. Alicea, G. Refael, F. von Oppen, K. Watanabe, T. Taniguchi, and S. Nadj-Perge, Nat. Phys., https://doi.org/10.1038/s41567-019-0606-5 (2019).
[75] C. Gutiérrez, C.-J. Kim, L. Brown, T. Schiros, D. Nordlund, E. B. Lochocki, K. M. Shen, J. Park, and A. N. Pasupathy, Nat. Phys. **12**, 950 (2016).